Thermal Response of Integral, Multicomponent Composite Thermal Protection Systems

David A. Stewart* and Daniel B. Leiser*
NASA Ames Research Center, Moffett Field, California
Paul Kolodziej†
Sterling Software, Palo Alto, California
and
Marnell Smith‡
NASA Ames Research Center, Moffett Field, California

Integral, multicomponent thermal protection materials are discussed in terms of their thermal response to an arc-jet airstream. In-depth temperature measurements are compared with predictions from a one-dimensional, finite difference code using calculated thermal conductivity values derived from an engineering model. The effect of composition, as well as the optical properties of the bonding material between the components, on thermal response is discussed. The performance of these integral, multicomponent composite materials is compared with the baseline Space Shuttle insulation.

Nomenclature

d = diameter, cm
H = enthalpy, MJ/kg
h = insulation thickness, cm
k = thermal conductivity, cal/cm^{-1}·s^{-1}·K^{-1}
k_W = reaction rate constant, cm/s
k' = unweighted thermal conductivity
L = pore size, cm
L_V = vehicle length, cm
l = fiber length, cm
N = number of fibers
P = pressure, atm
q = heat flux, W/cm^2
R = radius, cm
S_V = volume fraction
s = distance from vehicle nose, cm
T = temperature, K
t = time, s
x = distance from model surface, cm
α = angle of attack, deg
δ = cone half-angle, deg
ϵ_{TH} = total hemispherical emittance
λ = wavelength
ρ = density, g/cm^3
σ = tensile strength, dyn^e/cm^2
θ = angle between fibers, deg

Subscripts

e = boundary-layer edge
eff = effective
g = gas conduction
i = internal
M = engineering model
N = nose
o = stagnation point
r = radiation heat transfer
s = surface
so = solid conduction
st = strong direction
T = total
W = weak direction
X = in-depth
∞ = freestream conditions

Introduction

THE thermal-protection system (TPS) design requirements for spacecraft that re-enter the Earth's atmosphere using aerodynamic forces to decelerate and maneuver, such as an aeroassisted orbital transfer vehicle (AOTV) or advanced military spacecraft,[1-3] will be more demanding than those established for the Space Shuttle. These vehicles require TPS with high-temperature capability at the outer mold line (OML) and strong mechanical properties at the inner mold line (IML) near the stagnation point. This combination of properties can be achieved through an integral, multicomponent TPS in which two materials serving two different purposes are bonded together. Ideal candidates for this system are low-density fibrous refractory composite insulation (FRCI) and alumina enhanced thermal barrier (AETB),[4-5] since both can be tailored to meet the specific design requirements for an advanced vehicle TPS. For example, a wide range of mechanical properties can be obtained in FRCI by varying the weight percentage of silicon and aluminoborosilicate fibers in the composite; however, the temperature capability of FRCI is limited. Surface recession (linear shrinkage), a measure of temperature capability, can be minimized by adding alumina fibers to the FRCI composite to make AETB, but there is a loss in tensile strength. Therefore, a TPS without surface recession at high temperature and high tensile strength might be achieved by bonding an AETB to the front surface of a high strength FRCI.

In order to study the potential use of these multicomponent systems on any advanced vehicle, their thermal response to aerothermodynamic heating must be determined. The short duration heat pulse generated at the surface of these vehicles is transferred through the TPS by three mechanisms: solid and gas conduction and radiation heat transfer. Radiation heat transfer will play a major role in the determination of material thermal response because of the high temperatures associated with the aerobraking maneuvers of both types of vehicles. The thermal response of selected multicomponent TPS to an

Presented as Paper 85-1056 at AIAA 20th Thermophysics Conference, Williamsburg, VA, June 19-21, 1985; revision received Nov. 15,1985.

*Research Scientist.
†Research Engineer.
‡Research Technician.

aerothermodynamic arcjet environment was therefore studied at surface heating rates high enough to include radiation heat transfer within these materials. Thermal conductivity of each individual composite was determined using an engineering model and a thermal-response computer program.[6] These computations and arcjet data were used to accomplish the following:

1) Evaluate the thermal performance of multicomponent composite TPS in an aerothermodynamic environment.

2) Compare in-depth temperature data from these TPS with current Space Shuttle insulation.

3) Determine the effect of the bond-line emittance on the in-depth temperature response of these systems.

4) Illustrate the use of the engineering model thermal conductivity computations in evaluating the thermal response of a multicomponent composite TPS to an aerothermodynamic heating environment of a high-speed spacecraft during aerobraking maneuvers from geosynchronous orbit to low Earth orbit.

Background

Environment

Because of the low catalytic efficiency of reaction cured glass (RCG) coatings on these fibrous composites, the heating rate to both classes of high-speed vehicles would be minimized.[7] As an example, using previously derived reaction rates that characterize the surface-catalyzed recombination of atoms diffusing through the boundary layer to the TPS surface, the stagnation point heat transfer rate was calculated for reacting[8] and equilibrium boundary layer flows over a bent biconic during a descent from a geosynchronous orbit to a low Earth orbit (Fig. 1). In both computations, a total hemispherical emittance of 0.89 was used and it was assumed that time zero began at an altitude of 121 km. The heating pulse is relatively short (600 s). Its magnitude is roughly a third of the calculated values, assuming equilibrium boundary-layer flow or a fully catalytic wall. Surface temperature at the stagnation point will approach 2000 K. Therefore, the TPS near the nose of the vehicle will require materials that can withstand higher temperatures than the Space Shuttle reusable surface insulation, FRCI 12. A possible candidate is the integral multicomponent composite.

Materials

An integral, multicomponent TPS for advanced high speed vehicles will probably be bonded directly to a molded composite such as a polyimide/graphite structure.[9] This hard-bond TPS construction requires that the insulation have a low modulus and high tensile strength at the IML with high-temperature capability (resistant to shrinkage) at the OML. Development of low density FRCI and AETB materials have been directed at improving the resistance of these materials to damage and to increasing their temperature capability relative to that of the current Space Shuttle TPS.[10,11] The mechanical properties of FRCI, as well as some surface recession data, are plotted in Figs. 2 and 3. These data show that a wide range of mechanical properties can be obtained by varying the percentage of the aluminoborosilicate fibers and that the maximum tensile strength is obtained with 40% aluminoborosilicate fibers (Fig. 2). Increasing the weight percentage of aluminoborosilicate fibers beyond 40% reduces the FRCI surface recession rate, but also significantly reduces its tensile strength. The AETB material shows no surface recession at surface temperatures up to 1840 K, while maintaining a tensile strength equivalent to that of a silica insulation of the same density (Fig. 3). Therefore, combinations of existing low density fibrous composite insulations are currently available to meet many specific mechanical and physical property design requirements for the hard-bond TPS in the high temperature nose cap regions of these vehicles. Another critical design parameter that must be considered, however, when choosing the composite insulations for the multicomponent TPS, is the thermal conductivity.

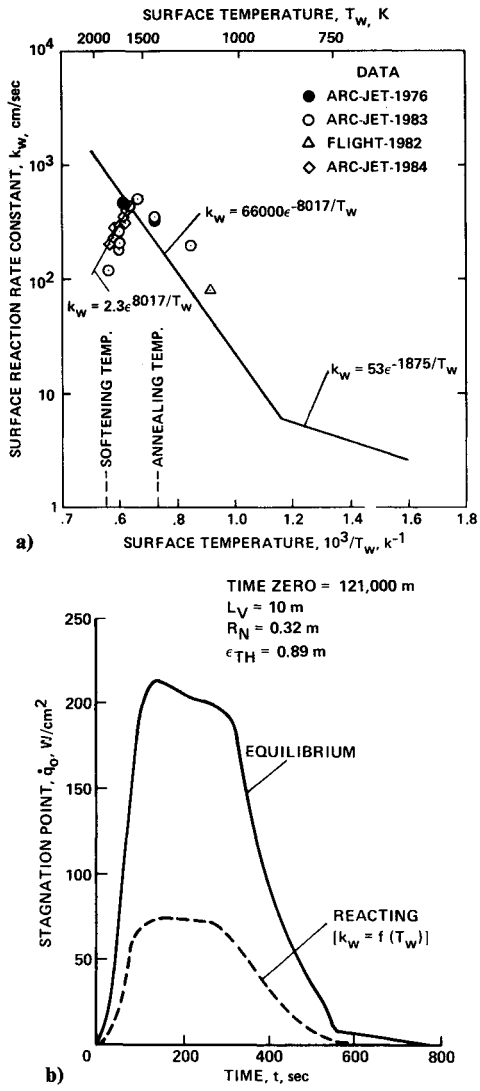

Fig. 1 Typical AOTV stagnation heating conditions. a) surface temperature dependence of the reaction rate constant for RCG coating; b) typical AOTV heating pulse.

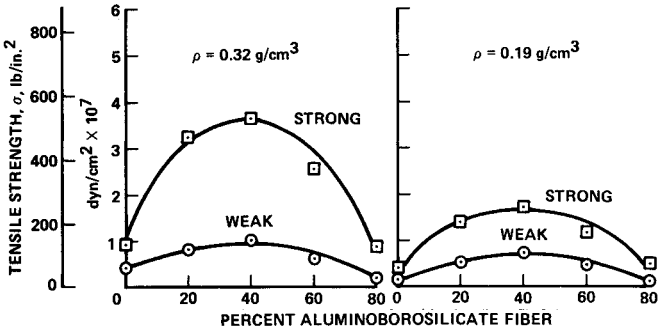

Fig. 2 Tensile strength of FRCI as a function of aluminoborosilicate fiber content.

Thermal Conductivity Model

In general, the thermal conductivity of fibrous insulations is determined from ASTM guarded hot-plate measurements[12] for temperatures up to 1350 K. These steady-state methods require homogeneous materials in the form of large flat slabs (18 cm in diameter) with smooth surfaces. In addition, the thermal gradient through the insulation must be known. Secondary methods for determining the steady-state thermal conductivity of insulating materials include using a comparative rod apparatus or a radial in-flow apparatus.[13,14] The radial in-

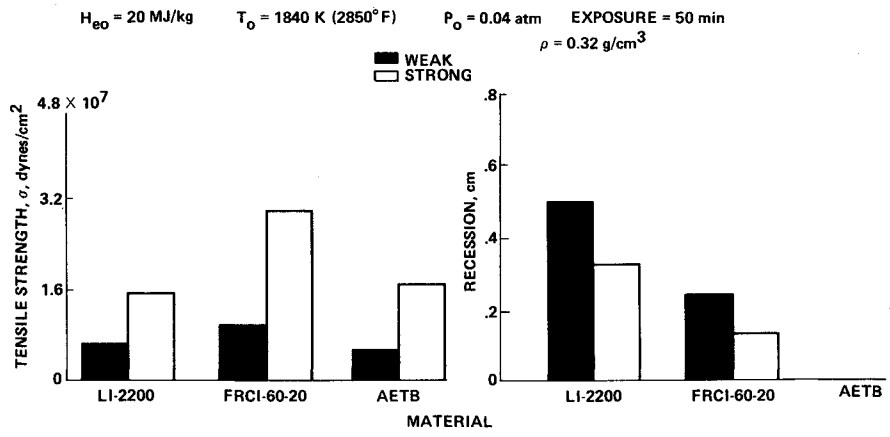

Fig. 3 Comparision of mechanical and thermal properties of composite insulations.

flow apparatus can extend the upper temperature limit to 3000 K, but it is limited to very small specimens and is of questionable accuracy because of errors associated with heat losses during measurements. The accuracy with which these methods can determine thermal conductivities in transient environments—where surface temperatures change rapidly—is limited. This is due in part to the larger role that radiation heat transfer plays in the overall temperature dependence of a material's thermal conductivity at high temperature.

During the Space Shuttle program, the effective thermal conductivity of a silica insulation was obtained from thermal-response data taken in an arcjet airstream used to simulate the short heating pulse (1200 s) over the Shuttle during Earth entry. These values were obtained by Curry and Williams[15] using an implicit thermal model to calculate the thermal response and nonlinear least-squares techniques to generate a polynomial expression for thermal conductivity as a function of temperature. Effective thermal conductivity for fibrous insulations can also be computed using a technique that iterates between an engineering model, finite difference thermal-response program and material in-depth temperature data obtained from an arcjet exposure.[16] Such a computation was made using data obtained from the Aerothermodynamic Heating Facility at Ames Research Center. A flow chart of this computation is shown in Fig. 4. Two parameters, which relate to variations in fiber bonding and optical properties of the composites, wer found to correlate with the physical properties of the engineering model.

The engineering model consists of interlocking walls of fibers that form uniform cubic pores (Fig. 5). The model is defined by governing equations relating composition and physical and mechanical properties of the actual complex fiber structure of the composites. Equations defining the pore size and fiber diameter in the model are

$$L_M = d_M/(S_V/3)^{1/2} \tag{1}$$

$$d_M = [S_v/\rho_T l_M]^{1/2} \tag{2}$$

Weak and strong directions of the composite are defined by tensile strength measurements, assuming that the number of fibers under load within the walls of the model is proportional to the tensile strength and angle between them. The anisotropic nature of these composites is included in the model by placing fewer fibers in the walls representative of the weak direction orientation of the insulation. The percentage of the total number of fibers in the weak direction can be calculated from

$$N_W/N_T = 2\sigma'_W/[2\tan(\theta/2)(1-\sigma'_W)+\sigma'_W] \tag{3}$$

where $\sigma_W = \sigma_W/\sigma_W + \sigma_{st}$. Assuming that the insulation is direc-

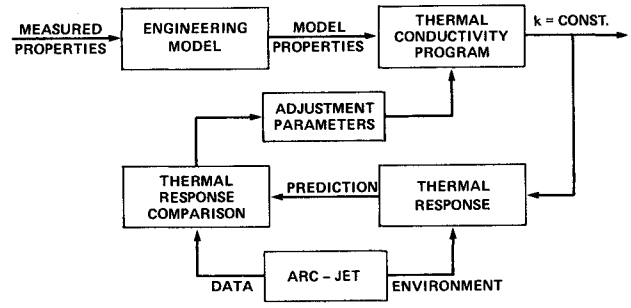

Fig. 4 Thermal conductivity computation flow chart.

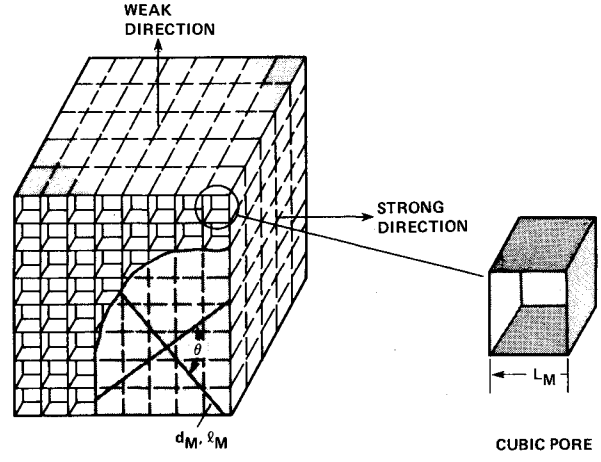

Fig. 5 Cubic pore engineering model.

tionally homogeneous, that it has uniform pores, and that heat is conducted in only one direction, the equations for solid and gas conduction and radiation heat transfer through the model are additive,

$$k = k_{so} + k_g + k_r \tag{4}$$

Applying the rule of mixtures and correcting for variations in fiber bonding η and optical properties β for each composite, Eq. (4) becomes

$$k = \eta(N_W/N_T)f_1(S_V)k'_{so} + (1-S_V)k'_g + f_2(S_V)\beta k'_r \tag{5}$$

where $f_1 = S_V$ and $f_2 = 1/S_V$. A detailed description of the equations for effective thermal conductivity of the individual

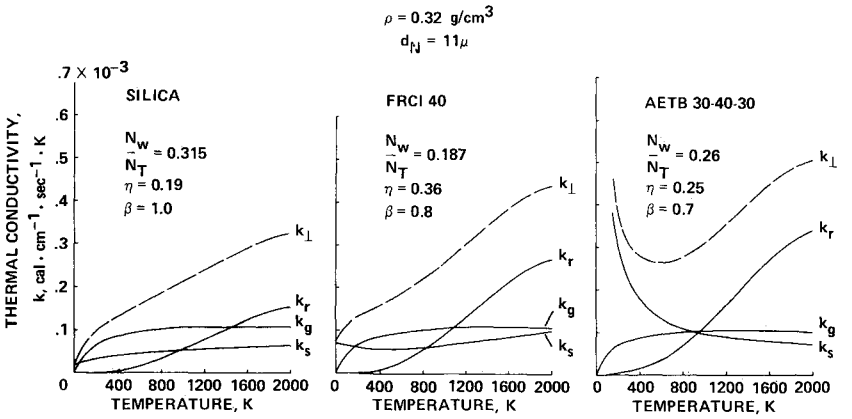

Fig. 6 Effect of composition on thermal conductivity.

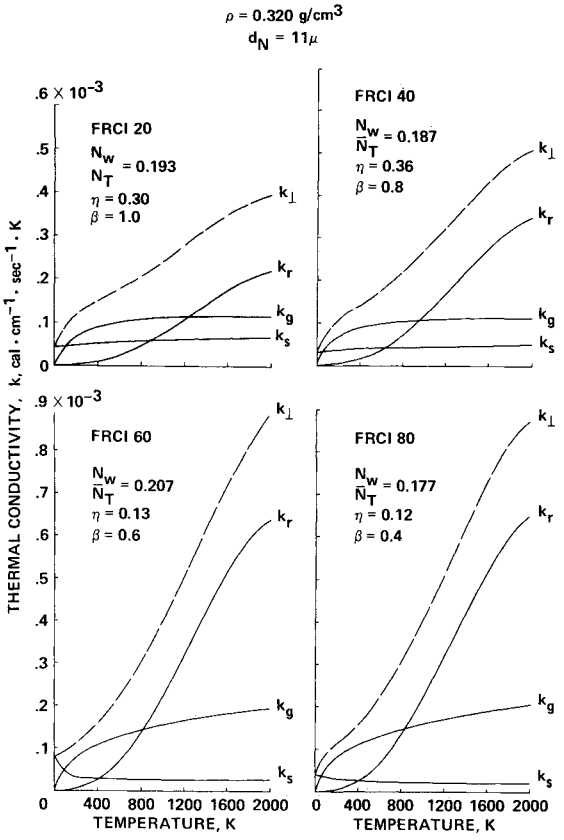

Fig. 7 Thermal conductivity for FRCI.

composite insulations is given in Ref. 6. Effective thermal conductivities for composite insulations obtained using this method are shown in Figs. 6 and 7. These computations show that the overall effective thermal conductivity profile is substantially influenced by radiation heat transfer k_r at high temperatures. The two adjustment parameters η and β, which relate to the solid conduction and radiation heat-transfer terms, were found to be independent of composition and fiber size and to depend only on the solid volume fraction and porosity (Fig. 8).

Facility

Arc-jet tests were conducted in the Ames Aerothermodynamic Heating Facility. This facility provides a high-energy airstream by passing air through a constricted arc-heater and expanding it through a 30 deg total-angle conical nozzle at Mach 5. Integral, multicomponent composite TPS are tested in the form of aerodynamic configurations such as a blunt cone. Surface conditions on the model are varied by changing the nozzle exit diameter, thus varying the pressure and the electrical power dissipation in the arc heater. The geometric area ratio of the nozzle exit to nozzle inlet was 400. The arrangement of the model and instrumentation in the test facility is shown in Fig. 9. The test model was mounted on a water cooled support strut that was driven by a worn gear in and out of the airstream. A 5.08 cm diam copper hemisphere, mounted on a swing-in arm containing a steady-state calorimeter and pressure port, was used to determine the stagnation point conditions for each test. A thermopile radiometer and a pyrometer were used to measure the stagnation point reradiation heat flux and surface temperature during each test. Barium fluoride and quartz windows were used with respective instruments to obtain maximum response over their operating range. Both instruments were calibrated using a blackbody radiation source and a standard micro-optical pyrometer ($\lambda = 0.65\ \mu$) with the tunnel windows in place.

Test Models

The models used in these arcjet tests were flat faced, 40 deg half angle cones (Fig. 10). The models consisted of a flat faced insert and a conical insulation ring. The insert had a face radius of 3.8 cm, an edge radius of 1.3 cm, and a thickness of 3.8 cm. It was made of two composite insulations bonded together with a 0.030 cm thick layer of glass adhesive. The front surface was coated with RCG. Six platinum-platinum/13% rhodium thermocouples (0.013 cm diam wire) were installed at various depths through the composites. They were installed just under and in contact with the RCG coating and glass bond, as well as at depths varying from $0.17 \leq x/h \leq 0.83$. A Chromel-constantan thermocouple (0.26 cm diam wire) was installed in the aluminum baseplate. The flat faced insert was fitted into a conical insulation ring 15.2 cm in diameter and 2.54 cm thick that was attached to a water-cooled strut.

The multicomponent composites TPS and their respective bonds used in these tests are listed in Table 1. The total hemispherical emittance for the various bond line materials were calculated from spectral/hemispherical reflectance and transmission data obtained from Perkin-Elmer model 330 and Willey 318 spectrophotometers. Both models 1 and 2 were made from silica. Models 3 through 5 were constructed with FRCI 20, FRCI 60, and AETB OMLs and FRCI 20 IMLs bonded together with a glass containing a tetraboron silicide emittance agent. Models 6 and 7 were constructed with FRCI 20 and FRCI 60 OMLs and FRCI 20 IMLs bonded together with a glass containing titanium oxide. Model 8 was constructed with an AETB OML and a FRCI 20 IML bonded with a transparent glass. The effective density of each of these multicomponent composites was 0.35 g/cm^3. The remaining

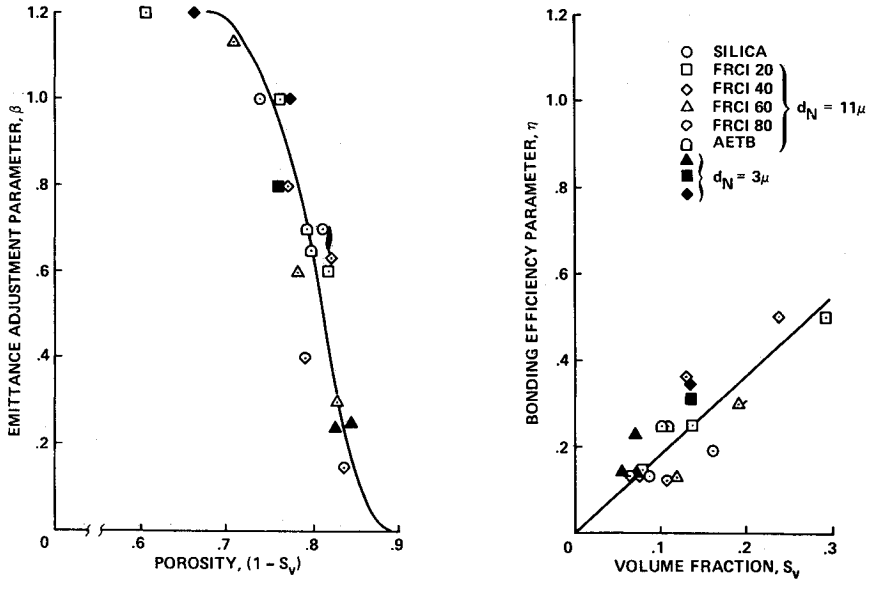

Fig. 8 Adjustment parameters for composite insulations.

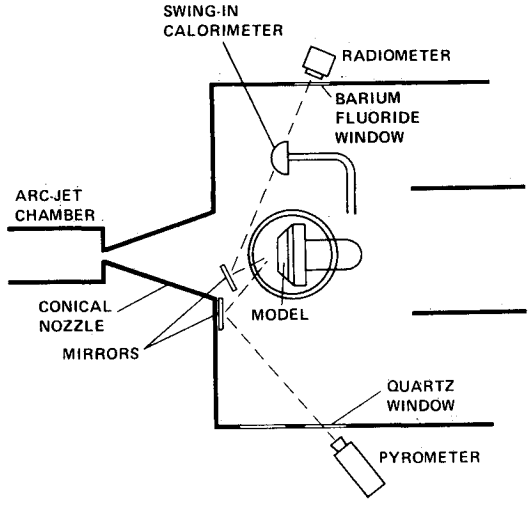

Fig. 9 Test facility.

two models, 9 and 10, were constructed with AETB OMLs and FRCI IMLs. Model 9 had a 0.17 g/cm^3 AETB composite bonded to a 0.19 g/cm^3 FRCI 15 IML with a glass containing the tetraboron silicide emittance agent. Model 10 had a 0.35 g/cm^3 AETB OML bonded to a 0.19 g/cm^3 FRCI 20 with a glass containing the titanium oxide.

Analysis and Experiment

During the present investigation, the thermal responses of these multicomponent composites were calculated by coupling the thermal response and thermal conductivity programs together. Material property inputs to the program included the composition of each composite, physical properties from the engineering model, and average values of η and β. Average values of η and β are represented by the faired curves through the data in Fig. 8.

Test environment inputs to the program were the stagnation point heat flux and enthalpy and internal model pressure histories. Stagnation point conditions for these tests were $\dot{q}_o = 40$ W/cm^2, $H_{eo} = 23.0$ MJ/kg, and $P_o = 0.02$ atm. The internal pressure P_i of the test models during the heating pulse was 0.01 atm. This is slightly less than a predicted value for the surface pressure on a 40 deg half-angle cone using modified Newtonian theory. The test environment consisted of a 300 s square-wave heating pulse followed by a cool-down of 600 s. The cool-down was conducted in a vacuum of 0.019 atm.

Results and Discussion

Arcjet data are compared with theory in Figs. 11-15. A predicted response for a thermocouple located just under and in contact with the RCG coating on the front surface of silica model 1 is compared with the data in Fig. 11. There is good agreement between the predicted and measured temperatures over both the heating and cool-down portions of the test environment. Similar results were also obtained for the other test models. Therefore, only the heating portion of the surface temperature time history was included with the in-depth temperature measurements shown in Figs. 12 and 13. The thermal response data from the silica model are compared with predictions made using both the thermal conductivity values obtained from guarded hot plate measurements[16] and the present engineering model techniques Fig. (12). In general, guarded hot plate conductivity values overpredicted the in-depth temperatures, whereas the prediction using the engineering model agree well with the data. The validity of the thermal response computation for these fibrous insulations was also evaluated by comparing in-depth temperature measurements from models 4 and 9 (Fig. 13). These data show good agreement with the predictions, even though their effective densities are $\rho_{\text{eff}} = 0.35$ and 0.21 g/cm^3.

Using temperature profiles instead of temperature time histories, the thermal response of multicomponent composite TPS (models 3-5) with FRCI 20 IMLS are compared with silica in Fig. 14. These data show that the system with FRCI 20 as the OML materials had the coolest response, AETB was roughly equivalent to silica, and FRCI 60 had the hottest response at 300 s. At 900 s, the bond line temperatures ($x/h = 0.33$) of all of the multicomponent composites were above the temperature of the silica at the same depth. The AETB OML composite bond line temperature was closer to that of the silica than were the other systems. The highest bond-line temperatures (1000 K) occurred in model 4 (FRCI 60). Predicted in-depth temperatures were in good agreement with the data, except at the back wall of the IML where the boundary conditions, specifically heat losses, could not be properly modeled in the thermal response program.

The effect of emittance of the bond line on in-depth temperature response was evaluated by comparing data from models 3-5 with data from models 6-8 (Fig. 15). Comparisons of the measured and predicted temperature profiles show good agreement. The bond line emittance was not included in the

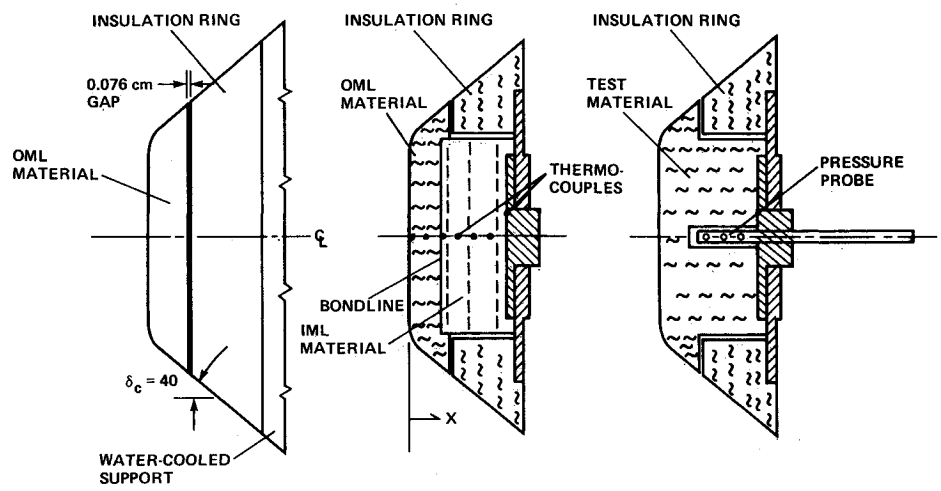

Fig. 10 Test models.

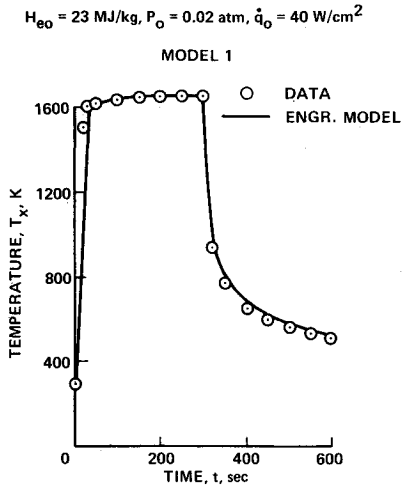

Fig. 11 Predicted and measured surface-temperature response of 40 deg blunt cone to an arcjet airstream.

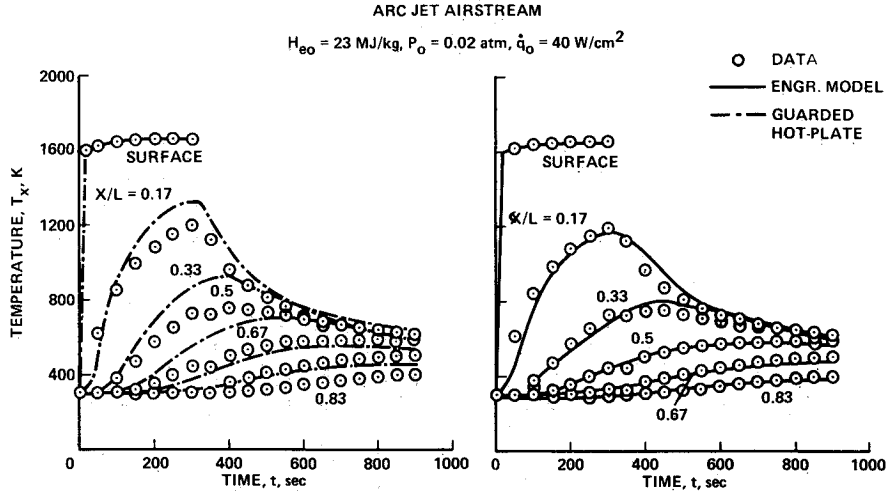

Fig. 12 Comparison of measured and predicted in-depth temperatures for silica.

Table 1 Multicomponent composite TPS models

Model	Bond line Agent	Bond line ϵ_{TH} 1000 K	OML	Density, g/cm^3	IML	Density, g/cm^3
1	–	–	SILICA	0.35	–	–
2	–	–	SILICA	0.35	–	–
3	SiB_4	0.89	FRCI 20	0.35	FRCI 20	0.35
4	SiB_4	0.89	FRCI 20	0.35	FRCI 20	0.32
5	SiB_4	0.89	AETB	0.35	FRCI 20	0.35
6	TiO_2	0.50	FRCI 20	0.35	FRCI 20	0.32
7	TiO_2	0.50	FRCI 60	0.35	FRCI 20	0.33
8	None	0.40	AETB	0.34	FRCI 20	0.34
9	SiB_4	0.89	AETB	0.17	FRCI 15	0.19
10	TiO_2	0.50	AETB	0.35	FRCI 20	0.19

[a]Pressure model.

prediction of the temperature profiles through these systems. These data show no appreciable effect of the bond line emittance on the in-depth temperature, even though the emittance varied from of 0.4 to 0.89.

Finally, utilizing a typical AOTV entry heating pulse (Fig. 1) for the stagnation point, the thermal response of a multicomponent composite TPS, consisting of an AETB ($\rho = 0.32$ g/cm^3) OML and FRCI 20 ($\rho = 0.19$ g/cm^3) IML, bonded to a graphite/polyimide structure (0.76 cm thick) was calculated (Fig. 16). The TPS had an effective density of $\rho_{eff} = 0.25$ g/cm^3. Thermal response of this TPS was estimated using the computational method outlined above for the test models. The assumptions used in the computation were an adiabatic back wall, low surface catalysis, and no convective cooling during soak out. Based on this computation, the TPS thickness required at the stagnation point is 2.0 cm. This includes an AETB thickness of 0.67 cm and an FRCI thickness of 1.33 cm. The computation shows that the bond line temperature reaches a maximum of 1440 K, well below the softening point of the glass bond, and the surface reaches a maximum

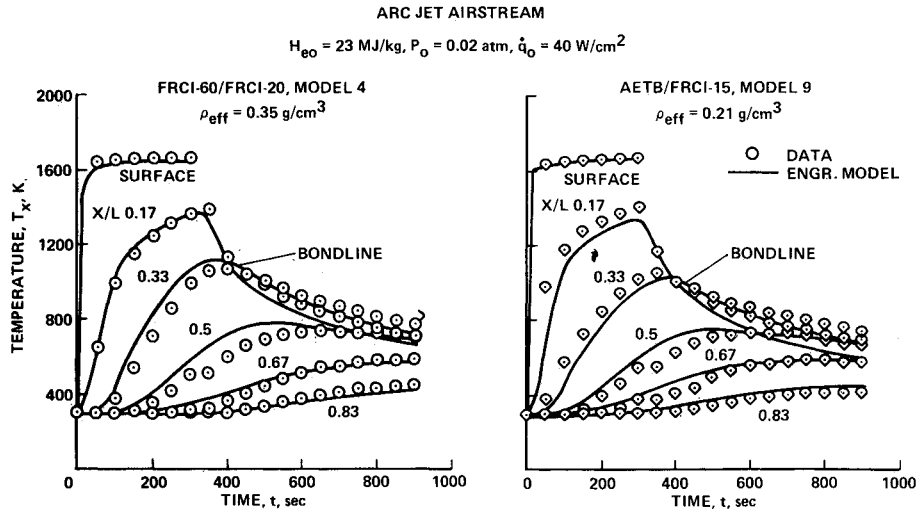

Fig. 13 Comparison of predicted and measured in-depth temperatures for multicomponent composite TPS.

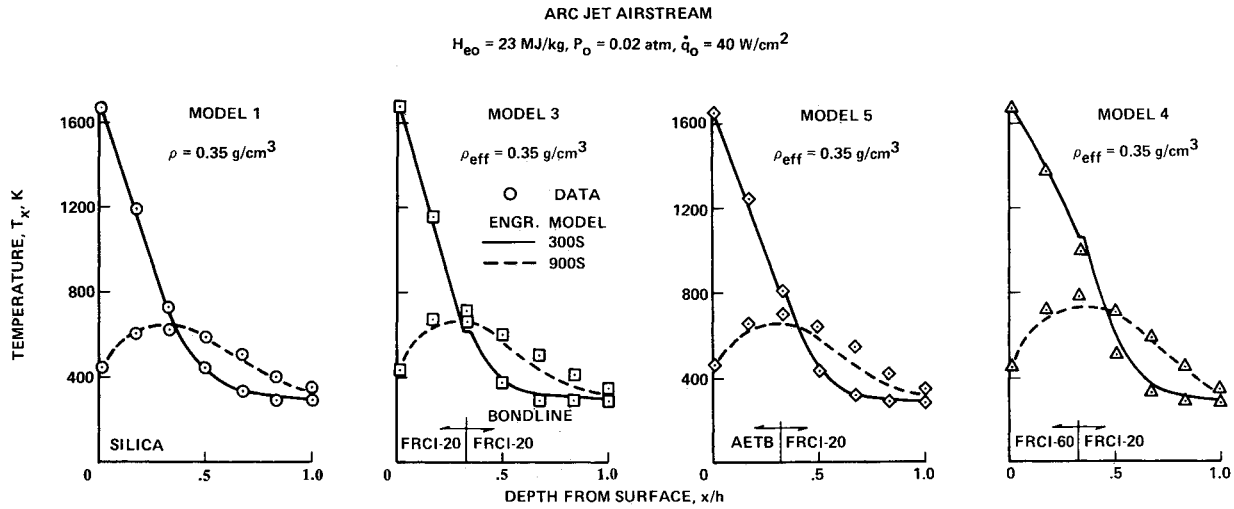

Fig. 14 Temperature profiles through various multicomponent composite TPS.

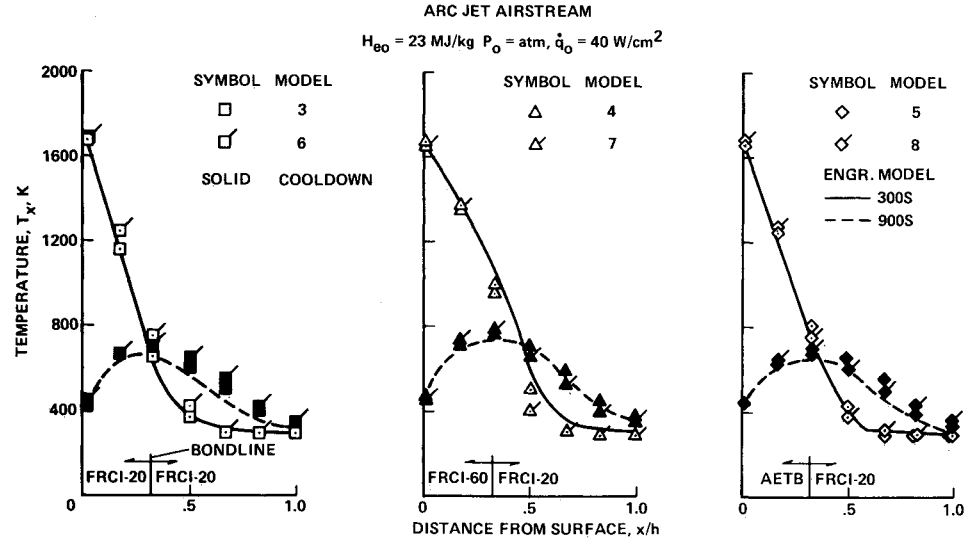

Fig. 15 Effect of bond line emittance on in-depth temperatures.

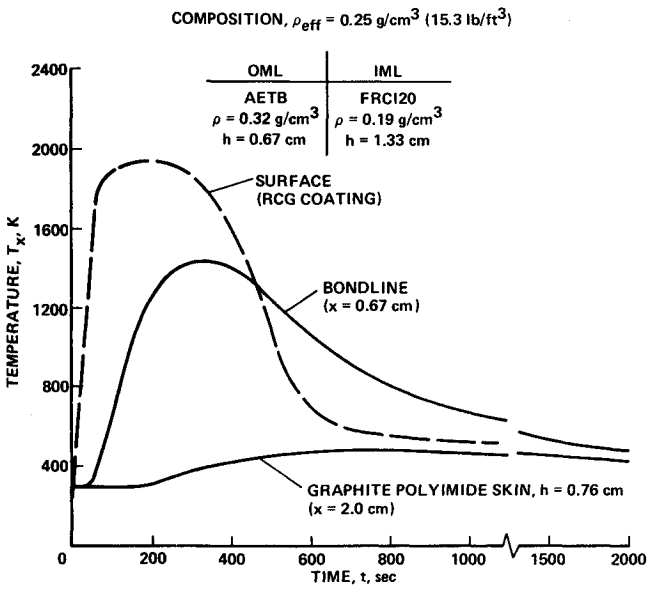

Fig. 16 Predicted thermal response of multicomponent composite TPS to stagnation point heating on a biconic during aerobraking maneuvers.

temperature of 1950 K. In previous tests,[10] one type of AETB did not shrink at a surface temperature of 1850 K during exposure to an arcjet airstream. The back wall temperature reached a maximum of 481 K, which is well under the maximum allowable (550 K) for the graphite/polyimide structure. A similar computation for a TPS that uses only AETB shows that a 20% increase in material density is required to obtain equivalent thermal performance to the integral multicomponent composite TPS just described. The above computation is not intended to be a design case for a AOTV, but only to illustrate the usefulness of the engineering model conductivity values as an aid in evaluating TPS performance on future high speed spacecraft during aerothermodynamic maneuvers in Earth's atmosphere.

Conclusions

The following conclusions were drawn from this investigation:

1) An engineering model and average values of adjustment parameters, relating to bonding and optical properties within individual composites, can be used to calculate the in-depth thermal response of multicomponent composites TPS.

2) The computation compares well with arcjet data for TPS systems made with composites having densities of 0.17-0.35 g/cm^3.

3) Bond-line emittance did not affect in-depth temperature response of these multicomponent composite TPS. However, higher in-depth temperature data are needed near the bond line to define the emittance effect more fully.

4) Integral multicomponent TPS are shown through thermal response computations to be feasible candidates for improving heat shield performance on vehicles associated with high-speed Earth entry or aerobraking manuever from geosynchronous to low Earth orbits.

Acknowledgments

The authors would like to acknowledge the excellent workmanship on the test models by both Victor Katvala and Thomas Hood of the NASA Ames Research Center.

References

[1]Gnoffo, P.A., "Complete Flowfields over Low and Wide Angle Conceptual Configurations," AIAA Paper 84-1695, 1984.

[2]Menees, G. P., "Thermal Protection Requirements for Near-Earth Aeroassisted Orbital Transfer Vehicle Missions," AIAA Paper 83-1513, 1983.

[3]Scott, C.D., et al., "Design Study of an Integrated Aerobraking Orbital Transfer Vehicle," NASA TM-58264, 1985.

[4]Leiser, D.B., Goldstein, H. E., and Smith, M., "Fibrous Refractory Composite Insulation," U.S. Patent 4, 148, 962, 1978.

[5]Leiser, D.B., Stewart, D.A., and Smith, M., "Rigidized Ceramic Heat Shield Materials for Advanced Space Vehicles," *Advances in TPS and Structures for Space Transportation Systems,* NASA CP-2315, 1983.

[6]Stewart, D.A. and Leiser, D.B., "Characterization of the Thermal Conductivity for Fibrous Refractory Composite Insulations," *Ceramic Engineering and Science Proceedings,* edited by W.J. Smothers, Vol. 6, No. 7-8, July-Aug. 1985, pp. 769-792.

[7]Stewart, D.A., Kolodziej, P., and Leiser, D.B., "Effect of Variable Surface Catalysis on Heating Near the Stagnation Point of a Blunt Body," AIAA Paper 85-0248, Jan. 1985.

[8]Rakich, J.V. and Lanfranco, M.J., "Numerical Computation of Space Shuttle Laminar Heating and Surface Streamlines," *Journal of Spacecraft and Rockets,* Vol. 14, May 1977, pp. 265-272.

[9]Riccitiello, S.R., Figueroa, H., Coe, C.F., and Kuo, C.P., "Advanced Leading Edge Thermal-Structure Concept—Direct Bond Reusable Surface Insulation to a Composite Structure," NASA TM-85941, 1984.

[10]Stewart, D.A., Leiser, D.B., and Smith, M., "Thermal Response of Advanced High Temperature Ceramic Composite Insulations to a Convectively Heated Environment," *Ceramic Engineering and Science Proceedings,* edited by W.J. Smothers, Vol. 4, No. 7-8, 1983, pp. 532-550.

[11]Leiser, D.B., Smith, M., and Stewart, D.A., "Thermal and Mechanical Properties of Advanced High Temperature Ceramic Composite Insulations," *Ceramic Engineering and Science Proceedings,* edited by W.J. Smothers, Vol. 4, No. 7-8, 1983, pp. 551-563.

[12]Standard Test Method for Steady-State Thermal Transmission Properties by Means of the Guarded Hot Plate (C 177-71), *Annual Book of ASTM Standards,* Pt. 18, ASTM, Philadelphia, PA, 1982.

[13]Engelke, W.T., "Suitable Steady-State Methods for Measurement of Effective Thermal Conductivity in Rigid Insulation," *Heat Transmission Measurements in Insulations,* STP544, ASTM, Philadelphia, PA, 1974, pp. 118-166.

[14]Pleanne, C.M., "Does the Insulation Have a Thermal Conductivity? The Revised ASTM Test Standards Require an Answer," *Thermal Transmission Measurements of Insulation,* STP660, ASTM, Philadelphia, PA, 1977, pp. 60-70.

[15]Curry, D.M. and Williams, S.D., "Nonlinear Least Squares—An Aid to Thermal Property Determination," *AIAA Journal,* Vol. 11, May 1973, pp. 670-674.

[16]"Thermal Protection System Materials Data," *Materials Properties Manual,* Rockwell International Shuttle Orbital Division, Space Systems Group, Downey, CA, Pub. 25430W, Rev. 5-79, Vol. 3, Dec. 1980.